



Supplementary Information for

Structural basis for antibiotic resistance mediated by the *Bacillus subtilis* ABCF ATPase VmlR

Caillan Crowe-McAuliffe, Michael Graf, Paul Huter, Hiraku Takada, Maha Abdelshahid, Jiří Nováček, Victoria Murina, Gemma C. Atkinson, Vasili Hauryliuk, Daniel N. Wilson

Daniel N. Wilson

Email: Daniel.Wilson@chemie.uni-hamburg.de

This PDF file includes:

Supplementary Materials and Methods
Figs. S1 to S7
Tables S1 and S2
References for SI reference citations

MATERIALS AND METHODS

Protein expression and purification

VmlR-EQ₂ in pET21b was synthesized by Eurofins. The resulting sequence encoded for a protein identical to GenBank record WP_003234144.1, except for the presence of an N-terminal hexahistidine tag and with glutamates 129 and 432 mutated to glutamines. *E. coli* BL21 (DE3) was used for protein expression. An 800 mL culture was grown at 37°C to OD₆₀₀ ~0.5, and protein expression was induced 1 mM IPTG for 5 h at 22°C. Cells were harvested at 8,000 × g for 10 min at 4°C. All subsequent steps were performed at 4°C or on ice. The pellet was washed with 50 mM sodium-phosphate (pH 8.0), 300 mM NaCl, and stored at -80°C. The pellet was thawed and resuspended in 30 mL buffer A (20 mM HEPES/KOH [pH 7.8], 200 mM NH₄Ac, 10 mM Mg(OAc)₂, 5 mM 2-mercaptoethanol) with 300 mM NaCl, protease inhibitor cocktail (Complete ultra EDTA-free, Roche), and 0.2 μL DNase I (Thermo). Cells were lysed with three passages through an EmulsiFlex-C3 cell homogeniser (AVESTIN, Inc, Ottawa, Canada) and the lysate was centrifuged at 15,000 × g for 10 min. Tween 20 was added to a concentration of 0.01% and the supernatant was applied to 0.5 mL pre-washed cobalt resin (TALON, Clontech). After binding for 90 min with gentle agitation, the resin was washed with 150 mL wash buffer (buffer A with 300 mM NaCl, 10 mM imidazole, and 5 mM 2-mercaptoethanol). Protein was eluted in 1 mL fractions with buffer A with 300 mM imidazole. Elution fractions 1-4 were centrifuged at 21,000 × g for 10 min, the supernatants pooled, and the resulting fraction purified by gel filtration over a HiPrep 16/600 75 pg column (GE Healthcare). The buffer used for gel filtration was buffer A supplemented with 0.5 mM EDTA. Elution fractions were centrifuged at 21,000 × g for 10 min, concentrated in a centrifugal concentrator (Ultra 4, 10 kDa MWCO, Amicon) and aliquots of the supernatant were snap-frozen in liquid N₂ and stored at -80°C.

Generation and purification of ErmDL-SRC

The ErmDL-SRC was generated based on the disome approach, as previously described (1, 2). The *2XermDL* construct contained a T7 promoter followed by a strong ribosome binding site (RBS) spaced by 7 nucleotides (nts) to the ATG start codon of the first *ermDL* cistron. A linker of 22 nts separated the stop codon of the first *ermDL* cistron and the start codon of the second *ermDL* cistron. The linker also comprised the strong RBS 7 nts upstream of the ATG start codon of the second *ermDL* cistron, enabling initiation of translation independent from the first *ermDL* cistron. With the exception of an R8K mutation, each *ermDL* cistron encoded amino acids 1-14 corresponding to the ErmDL leader peptide (Entry code P62188) present on the macrolide resistance plasmid pE194. The complete sequence of *2XermDL* construct is: 5'-*TAATACGACTCACTATAGGGAGTTTTATAAGGAGGAAAAAATATGACACACTC AATGAGACTTAAAGTTCCCAACTTTGAACCAGTAAAGTTTTATAAGGAGGAAA* AAATATGACACACTCAATGAGACTTAAAGTTCCCAACTTTGAACCAGTAA-3' (T7 promoter, italics; RBS, bold; ErmDL ORF, shaded grey with CTT codon in P-site of stalled ribosome shown in bold; annealing site for complementary DNA oligonucleotide, underlined).

In vitro translation of the *ermDL* construct was performed using purified *Bacillus subtilis* 70S and the PURExpress delta ribosome Kit (NEB). Translation reactions were

analyzed on sucrose density gradients (10-55% sucrose in buffer containing 50 mM HEPES-KOH, pH 7.4, 100 mM KOAc, 25 mM Mg(OAc)₂, 6 mM β-mercaptoethanol, 100 μM telithromycin and 1x Complete EDTA-free Protease Inhibitor cocktail (Roche)) by centrifugation at 154,693 × g (SW-40 Ti, Beckman Coulter) for 3 h at 4°C. For ErmDL-SRC purification, disome fractions were collected using a Gradient Station (Biocomp) with an Econo UV Monitor (Biorad) and a FC203B Fraction Collector (Gilson). Purified ErmDL-SRC disomes were concentrated by centrifugation at 88,760 × g for 4 h at 4°C (TLA120.2 rotor, Beckman Coulter). To obtain monosomes of the ErmDL-SRC, a short DNA oligonucleotide (5'-ttctcctataaaaact-3', Metabion) was annealed to the linker between the *ermDL* cistrons, generating a DNA-RNA hybrid that could be cleaved by RNase H (NEB) treatment in buffer A at 25°C for 1 h. After cleavage of the disomes, ErmDL-SRC monosomes were again purified and concentrated by centrifugation at 88,760 × g for 4 h at 4°C (TLA120.2 rotor, Beckman Coulter).

Grid preparation

Samples containing 2.5 pmol ErmDL-SRC, 12.5 pmol VmlR-EQ₂, 100 μM ATP, 10 μM telithromycin were prepared in 20 μL of buffer B (20 mM HEPES/KOH [pH 7.8], 100 mM NH₄Ac, 10 mM Mg(OAc)₂, 5 mM 2-mercaptoethanol). N-dodecyl β-D-maltoside was added to a final concentration of 0.1 % (v/v). (The final reaction contained 0.035% DMSO from the telithromycin stock). Reactions were incubated for 15 min at 22°C and then held at 4°C as samples were applied to 2 nm precoated Quantifoil R3/3 holey-carbon-supported grids and vitrified using a Vitrobot Mark IV (FEI, Netherlands).

Data collection and Processing

Images were collected with a Titan Krios TEM equipped with a Falcon III direct electron detector (FEI, Netherlands) at 300 kV using a pixel size of 1.061 Å and an under-defocus range of -0.8 to -1.6 μm. Micrographs were recorded as 39 frames, each with a dose of 1.425 e⁻/Å². Micrographs were aligned and dose-weighted with MotionCor2 (3) and the CTF of every micrograph was determined using GCTF (4). Template-free particle picking was performed using Gautomatch (<http://www.mrc-lmb.cam.ac.uk/kzhang/>) resulting in 286,701 particles. Manual inspection of thrice-decimated particle after 2D classification resulted in 159,722 particles that were further used for 3D-refinement using an *E. coli* ribosome filtered to 70 Å as an initial reference. The resulting volume was used as a reference for 3D classification yielding four different classes. The class containing VmlR and P-tRNA was subjected to focused sorting, using a spherical mask encompassing the P- and E-sites. Volumes of interest were then refined using undecimated particles. Final reconstructions were corrected for the modulation transfer function and sharpened by applying a negative B-factor estimated by RELION-2.1 (5). The average resolution of reconstructions was determined using the “gold-standard” criterion (FSC = 0.143) (6). ResMap was used for local resolution estimation (7). The final volumes were locally filtered using SPHIRE (8).

Modelling

A homology model of VmlR was created using the deposited structure of ABCF protein EttA (PDB ID 3J5S) (9) as a template for SWISS-MODELLER (10). The homology model was fitted into density with UCSF Chimera (11) using the command ‘fit in map’,

and manually adjusted with Coot (12). The well-resolved ARD helices could be modelled *de novo*, while residues 486–547 of the CTE of VmlR were modelled as polyalanine. The model of the *B. subtilis* 70S ribosome was derived from PDB ID 3J9W (13). For the less well resolved L1 protein, a homology model was created based on the *E. coli* L1 protein (PDB ID 5AFI) (14) using SWISS-MODELLER (10). The resulting model was rigid body fitted into the cryo-EM density using UCSF Chimera (11). ATP molecules and the *E. coli* Leu-tRNA were obtained from PDB ID 6BHU (15) and PDB ID 4WSM (16), respectively, and subjected to refinement as necessary. The atomic coordinates were refined using phenix.real_space_refine (17) with restraints obtained by phenix.secondary_structure_restraints (17). Statistics for the model were obtained using Molprobrity (18).

Figure preparation

Figures showing atomic models and electron densities were generated using either UCSF Chimera (11) or PyMol Molecular Graphic Systems (Schrödinger) and assembled with Adobe Illustrator. Growth curves were prepared with Igor Pro.

Construction of *B. subtilis* strains

Strain VHB5 [*trpC2* Δ *vmlR*] was constructed using the marker-free deletion technique (19) with wild type *B. subtilis* strain 168. First, three linear \approx 500 nt-long DNA fragments were amplified by PCR using genomic DNA as a template: one located upstream of the *vmlR* ORF (primers VmlR-A-F and VmlR-A-R; see **Table S2** for sequences), one downstream of the *vmlR* ORF (primers VmlR-B-F and VmlR-B-R) and one within the *vmlR* ORF (primers VmlR-C-F and VmlR-C-R). Second, the TMO310 *mazF* cassette was amplified by PCR using primers chpA-R and pAPNC-F. The cassette contains i) the *mazF* toxin ORF under the control of an IPTG-inducible promoter (P_{spac}), ii) the *lacI* ORF for expression of Lac repressor controlling the P_{spac} , and iii) the spectinomycin resistance marker (*spc*). All four PCR products described above were used simultaneously as the template for PCR amplification using primers VmlR-A-F and VmlR-C-R. The resultant long PCR fragment was used to transform the *B. subtilis* strain 168. *vmlR* deletion mutants were selected by spectinomycin resistance, followed by a second selection step on IPTG plates to identify marker-less *vmlR* deletion mutants lacking the *mazF* toxin ORF, yielding the VHB5 strain.

To construct the VHB44 [*trpC2* Δ *vmlR* *thrC*:: $P_{hyspnak}$ -*vmlR* *kmR*] strain untagged VmlR under the control of an IPTG-inducible *Phy-spank* promoter, a PCR product encoding *vmlR* was PCR-amplified from the VHp62 plasmid (pAPNC-*vmlR*-HTF) using the primers PhyvmlR_F and PhyvmlR_R. The second PCR fragment encoding a kanamycin-resistance marker, a polylinker downstream of the *Phy-spank* promoter and the *lac* repressor ORF – all inserted in the middle of the *thrC* gene – was PCR-amplified from pHT009 plasmid using primers pHT002_F and pHT002_R. The two fragments were ligated using the NEBuilder HiFi DNA Assembly master mix (New England BioLabs, Ipswich, MA) yielding the pHT009-*vmlR* plasmid which was used to transform the VHB5 [*trpC2* Δ *vmlR*] strain. Selection for kanamycin resistance yielded the desired VHB44 strain.

A QuikChange Multi Site-Directed Mutagenesis Kit (Agilent Technologies) was used to mutate the *vmlR* gene expressed from the pHT009-*vmlR* plasmid. Sequences of

the primers used to generate plasmids pHT009-*vmlRF237A* (F237A), pHT009-*vmlRF237V* (F237V), and pHT009-*vmlRΔCTE* (491STOPx2) are provided in the **Table S2**. To generate pHT009-*vmlRΔCTE*, two consecutive stop codons (TGATAA) were introduced after codon 491 (GAA). VHB5 [*trpC2 ΔvmlR*] strain was transformed with the plasmids listed above yielding upon selection for kanamycin resistance strains [*trpC2 ΔvmlR thrC::P_{hyspnak}-vmlRF237A kmR*], VHB89 [*trpC2 ΔvmlR thrC::P_{hyspnak}-vmlRF237V kmR*], and VHB88 [*trpC2 ΔvmlR thrC::P_{hyspnak}-vmlRΔCTE kmR*].

Antibiotic sensitivity testing

B. subtilis strains were pre-grown on LB plates either supplemented with 1 mM IPTG (VHB44 strain) or lacking the inducer (wt 168 and VHB5 strains) overnight at 30°C. Fresh individual colonies were used to inoculate filtered LB medium in the presence and absence of 1 mM IPTG, and OD₆₀₀ adjusted to 0.01. The cultures were seeded on a 100-well honeycomb plate (Oy Growth Curves AB Ltd, Helsinki, Finland), and plates incubated in a Bioscreen C (Labsystems, Helsinki, Finland) at 37°C with continuous medium shaking. After 90 min (OD₆₀₀ ≈ 0.1), antibiotics were added and growth was followed for an additional 6 hours.

Sequence alignments

To compare the sequence of the ARD domain among VmlR orthologs and other ABCF AREs, we generated a multiple sequence alignment using MAFFT v7.164b (20). VmlR-like proteins in the ARE2 family of ABCFs were retrieved from the ABCF database (21); VgaALC, LsaA, SalA, MsrE and OptrA were downloaded from The Comprehensive Antibiotic Resistance Database (CARD) (22), and EttA from Uniprot (23).

		$\alpha 1$	Phe237	$\alpha 2$	
VmlR <i>Bacillus subtilis</i>	183	GNYSGYMKFREKKRLTQQREY EKQQKMVERIEAQMNGLASWSEK	----	---AHAQS---TKKEG	-----
VmlR <i>Bacillus infantis</i>		GNYSYMEARRQKRLAQREY EKQQKMVERIEGQLNELSSWANT	----	---GHAQS---MKKEG	-----
VmlR <i>Bacillus macauensis</i>		GNYSYMEARRQKRLAQREY EKQQKMVERIEGQLNELSSWANT	----	---GHAQS---MKKEG	-----
VmlR <i>Planococcus antarcticus</i>		GNYSYMEARRQKRLAQREY EKQQKMVERIEGQLNELSSWANT	----	---GHAQS---MKKEG	-----
VmlR <i>Bacillus cereus</i>		GNYSYMEARRQKRLAQREY EKQQKMVERIEGQLNELSSWANT	----	---GHAQS---MKKEG	-----
VmlR <i>Bacillus atrophaeus</i>		GNYSYMEARRQKRLAQREY EKQQKMVERIEGQLNELSSWANT	----	---GHAQS---MKKEG	-----
VmlR <i>Bacillus bogoriensis</i>		GNYSYMEARRQKRLAQREY EKQQKMVERIEGQLNELSSWANT	----	---GHAQS---MKKEG	-----
VgaA _{LC} <i>Staph. haemolyticus</i>		GNYSNYVEQKELERHREELEYEKYEKKEKRLKAINIKEQKAQR	----	---ATKKPKNLSSEGKI	---
LsaA <i>Enterococcus faecalis</i>		GNFSIYEEQKLRDAFELAEENEKIKKEVNRLKETARKKAWSMN	----	---REGDKYGNKKEKSG	---
SalA <i>Staphylococcus sciuri</i>		GKYDKYKQKDI EHE TLK LQY EKQQKEAAIEETIKKYKAWYQK	----	---AEQSA	---
MsrE <i>Escherichia coli</i>		GGYS DYLRQKEEERQH QAVEYELMMKERERLES AVQEK RQQANRLDNKKKGEKSKNSTESAGRLGHAKMT	----	---GTRKRLYQAASMEKRLAA	---
OptrA <i>Enterococcus faecalis</i>		GNYSAFEEQKRENHIKQKDYDLQOIEIERITRLIERF	----	---	---
EttA <i>Escherichia coli</i>		GNYSWLE-QKDQRLAQEASQEAARR--KSIEKEL	----	---	---

Streptogramin A, lincosamides, pleuromutilins

Streptogramin B, macrolides

Phenicol, oxazolidinones

Translation factor

Figure S1. Sequence alignment of selected ARE-ABCF proteins. VmlR, a selection of uncharacterized proteins closely related to vmlR, as well as other AREs with known specificities, were aligned with MAFFT as described in the methods. A portion of an alignment spanning the interdomain linker region was selected for analysis. Helices $\alpha 1$ and $\alpha 2$ and Phe237 from *Bacillus subtilis* VmlR are indicated. Accession identifiers for sequences from top to bottom: *Bacillus subtilis* VmlR (Uniprot P39115), *Bacillus infantis* NRRL B-14911 (NCBI YP_008607708.1), *Bacillus macauensis* ZFHKF-1 (NCBI WP_007203347.1), *Planococcus antarcticus* DSM 14505 (NCBI WP_006828374.1), *Bacillus cereus* m1293 (NCBI WP_000675965.1), *Bacillus atrophaeus* 1942 (NCBI YP_003971957.1), *Bacillus bogoriensis* ATCC BAA-922 (NCBI WP_026673438.1), VgaA_{LC} [*Staphylococcus haemolyticus*] (CARD gb|ABH10964.1), MsrE [*Escherichia coli*] (CARD gb|YP_724476.1), LsaA [*Enterococcus faecalis*] (CARD gb|AAT46077.1), SalA [*Staphylococcus sciuri* subsp. *sciuri*] (CARD gb|AGN74946), OptrA [*Enterococcus faecalis*] (CARD gb|AKA86814)

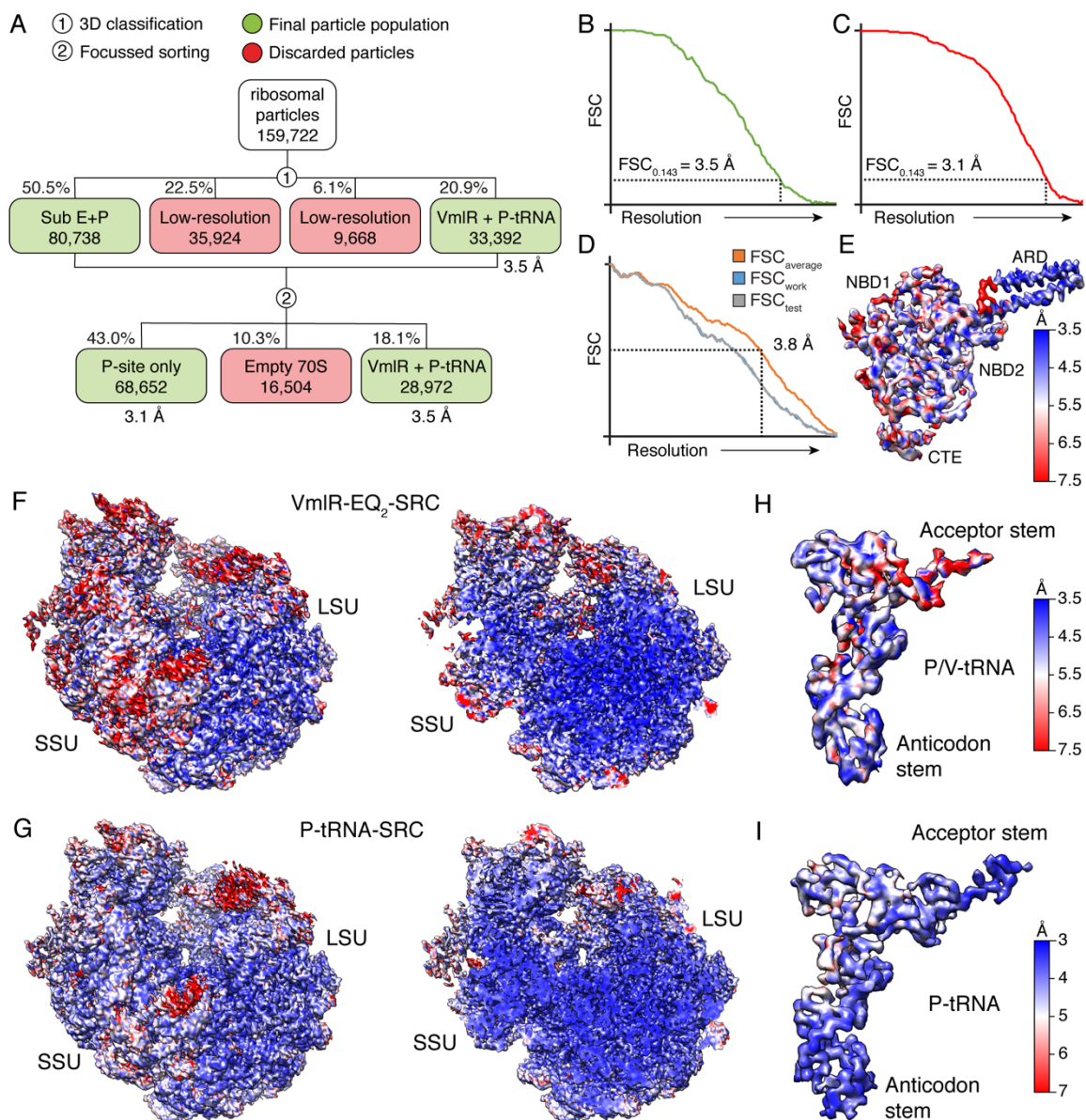


Figure S2. Processing of the cryo-EM data of VmlR-ribosome complex. (A) Following 2D classification, 159,722 ribosomal particles were subjected to 3D classification, sorting the particles into four distinct classes, with one defined population containing VmlR and P/V-tRNA (20.9%, 33,392 particles), a population with substoichiometric P-tRNA and two poorly resolved subpopulations that were discarded (red). Focused sorting was implemented yielding three classes, one bearing P-tRNA only (60.2%, 68,652 particles), one vacant 70S class (14.5%, 16,504 particles) and a defined population containing VmlR and P/V-tRNA (25.4%, 28,972 particles). (B-C) Fourier Shell Correlation ($FSC_{0.143}$; green) of the (B) VmlR-SRC (green) and (C) P-tRNA-SRC (red), with the resolution at $FSC=0.143$ indicated with a dashed line (D) $FSC_{average}$ (orange) and self and cross-validated correlations FSC_{work} (red) and FSC_{test} (green), respectively, shown for VmlR-70S complex. (E) Isolated density of VmlR from the cryo-EM map of the VmlR-ribosome complex colored according to local resolution. (F) Overview and (G) transverse section of the cryo-EM map of the VmlR-SRC colored

according to local resolution. **(H-I)** Isolated density of **(H)** P/V-tRNA from the VmlR-SRC and **(I)** P-tRNA from the P-tRNA-SRC colored according to local resolution. **(A)** Following 2D classification, 159,722 ribosomal particles were subjected to 3D classification, sorting the particles into four distinct classes, with one defined population containing VmlR and P/V-tRNA (20.9%, 33,392 particles), a population with substoichiometric P-tRNA and two poorly resolved subpopulations that were discarded (red). Focused sorting was implemented yielding three classes, one bearing P-tRNA only (60.2%, 68,652 particles), one vacant 70S class (14.5%, 16,504 particles) and a defined population containing VmlR and P/V-tRNA (25.4%, 28,972 particles). **(B-C)** Fourier Shell Correlation ($FSC_{0.143}$; green) of the **(B)** VmlR-SRC (green) and **(C)** P-tRNA-SRC (red), with the resolution at $FSC=0.143$ indicated with a dashed line **(D)** $FSC_{average}$ (orange) and self and cross-validated correlations FSC_{work} (red) and FSC_{test} (green), respectively, shown for VmlR-70S complex. **(E)** Isolated density of VmlR from the cryo-EM map of the VmlR-ribosome complex colored according to local resolution. **(F)** Overview and **(G)** transverse section of the cryo-EM map of the VmlR-SRC colored according to local resolution. **(H-I)** Isolated density of **(H)** P/V-tRNA from the VmlR-SRC and **(I)** P-tRNA from the P-tRNA-SRC colored according to local resolution.

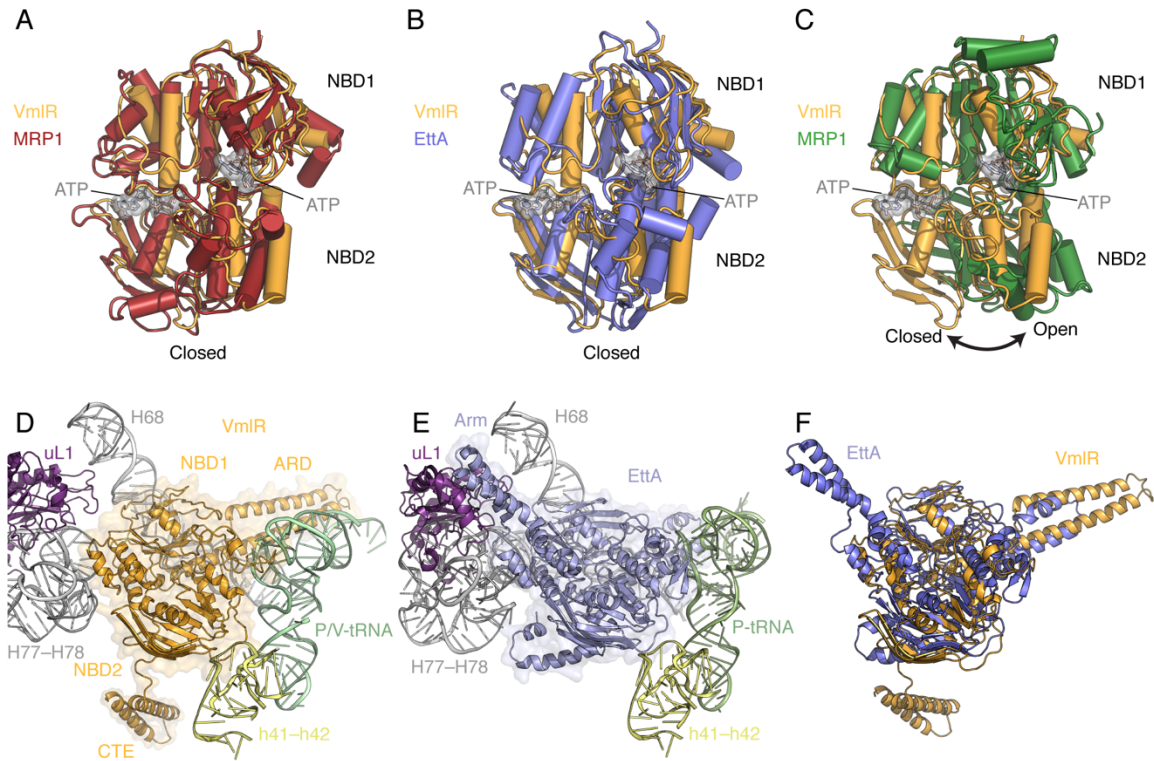


Figure S3. Conformation of the VmlR NBDs with respect to other ABC proteins. (A-C) Alignment (based on NBD1) of the closed conformation ABC domains of VmlR (orange) with (A) the closed conformations of multi-drug transporter MRP1 (red, PDB ID 6BHU) (15), (B) EttA (blue, PDB ID 3J5S) (9) as well as (C) the open conformation observed for ABCE1 (green, PDB ID 5LL6) (24). (D-F) Comparison of the binding site of VmlR (D) and EttA (E) on the ribosome. (F) Superimposition of ribosome-bound VmlR (orange) and EttA (blue) from (D) and (E), respectively.

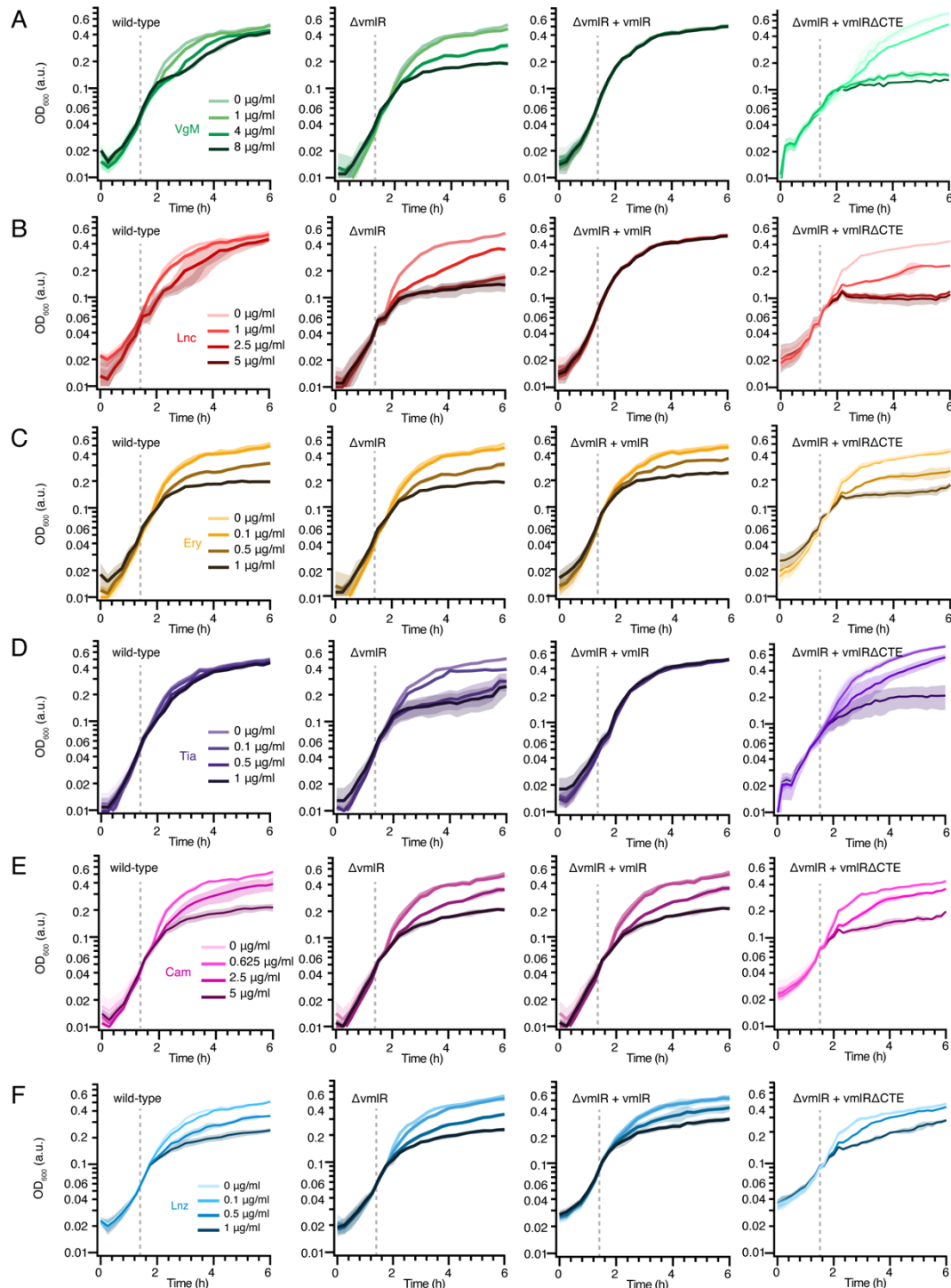


Figure S4. Antibiotic resistance conferred by VmlR and VmlRACTE *in vivo*. (A-F) Growth curves of wild-type *B. subtilis*, *vmlR*-knockout ($\Delta vmlR$) alone, and complemented by wildtype VmlR ($\Delta vmlR + vmlR$) VmlR- Δ CTE grown in the presence of increasing concentrations of (A) virginiamycin M1 (VgM), (B) lincomycin (Lnc), (C) erythromycin (Ery), (D) tiamulin (Tia), (E) chloramphenicol (Cam) and (F) linezolid (Lnz). Cells were diluted to an OD₆₀₀ value of 0.01 and grown in LB (with IPTG for the

complemented cells) at 37°C with shaking. After 90 minutes antibiotics were added at the indicated concentrations (dashed line) and growth was measured for a further 6 h.

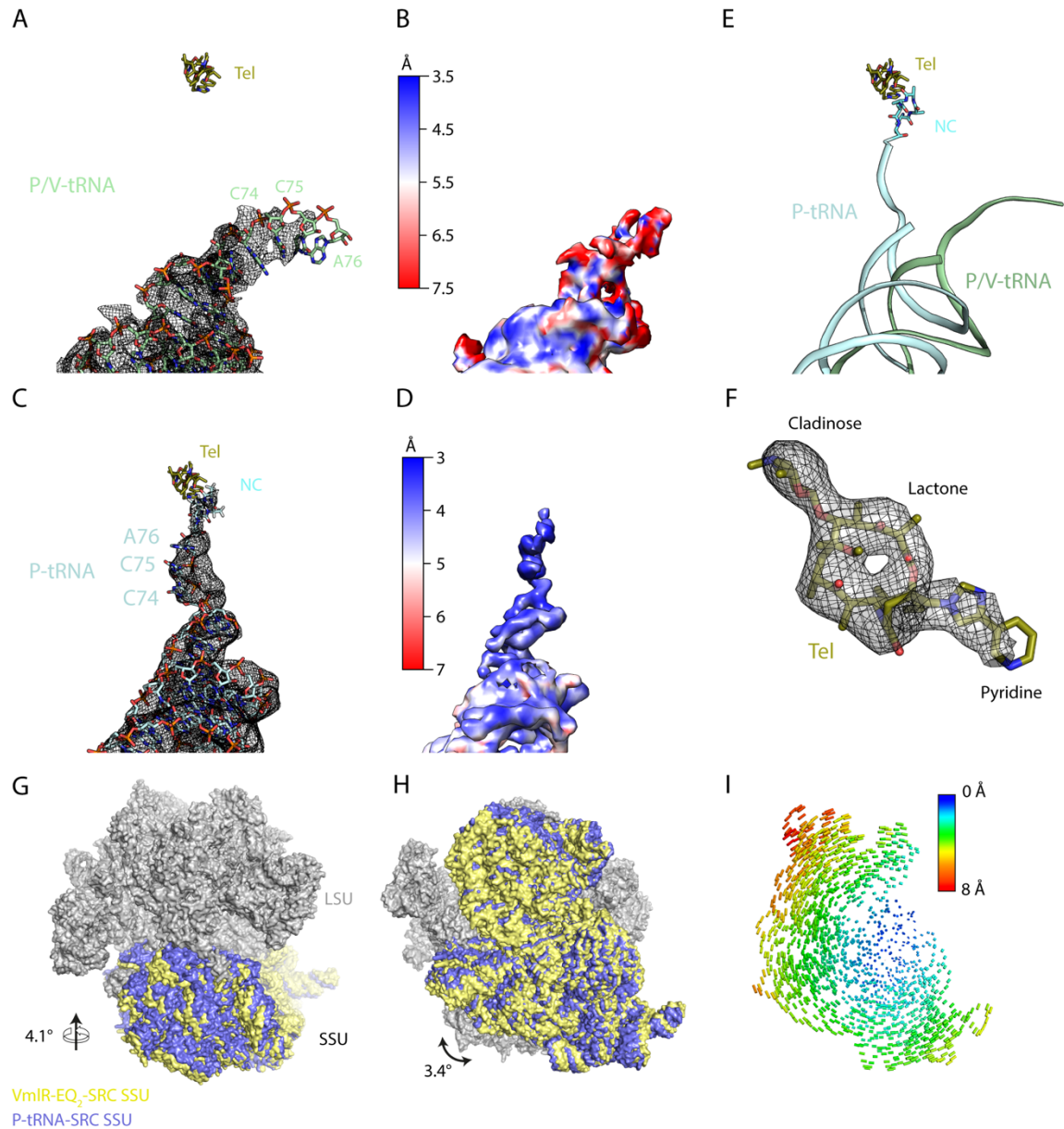


Figure S5. VmlR induces a P/V-site tRNA and subunit rotation. (A) Isolated cryo-EM electron density (grey mesh) for the P/V-tRNA (model in green sticks) from the VmlR-EQ₂-SRC. (B) Isolated cryo-EM electron density for the P/V-tRNA, as in (A), but coloured according to local resolution. (C) Isolated cryo-EM electron density (grey mesh) for the P-tRNA (model in cyan sticks) and ErmDL nascent chain (NC model in cyan sticks) from the P-tRNA-SRC. (D) Isolated cryo-EM electron density for the P-tRNA, as in (C), but colored according to local resolution. (E) Superimposition of P/V-tRNA (green ribbon) and ErmBL nascent chain (cyan) with P-tRNA (cyan ribbon). In (A-E), the binding site of telithromycin (Tel) is shown for reference. (F) Isolated cryo-EM electron density (grey mesh) for telithromycin (Tel, khaki sticks) from the P-tRNA-SRC, with cladinose, lactone ring and pyridine heterocycle indicated. (G-H) Alignment based on the LSU (grey) of the structures of the VmlR-EQ₂-SRC (SSU, yellow) and P-tRNA-SRC (blue) revealing a (G) 4.1° swivel of the SSU head and (H) 3.4° rotation of the SSU

body. **(I)** Illustration of movement of the SSU between the VmlR-EQ2-SRC and P-tRNA-SRC. The length and color of the lines correspond to the degree of movement between each phosphate group in of the SSU between the VmlR-EQ2-SRC and P-tRNA-SRC structures. The view is the same as in **(H)**.

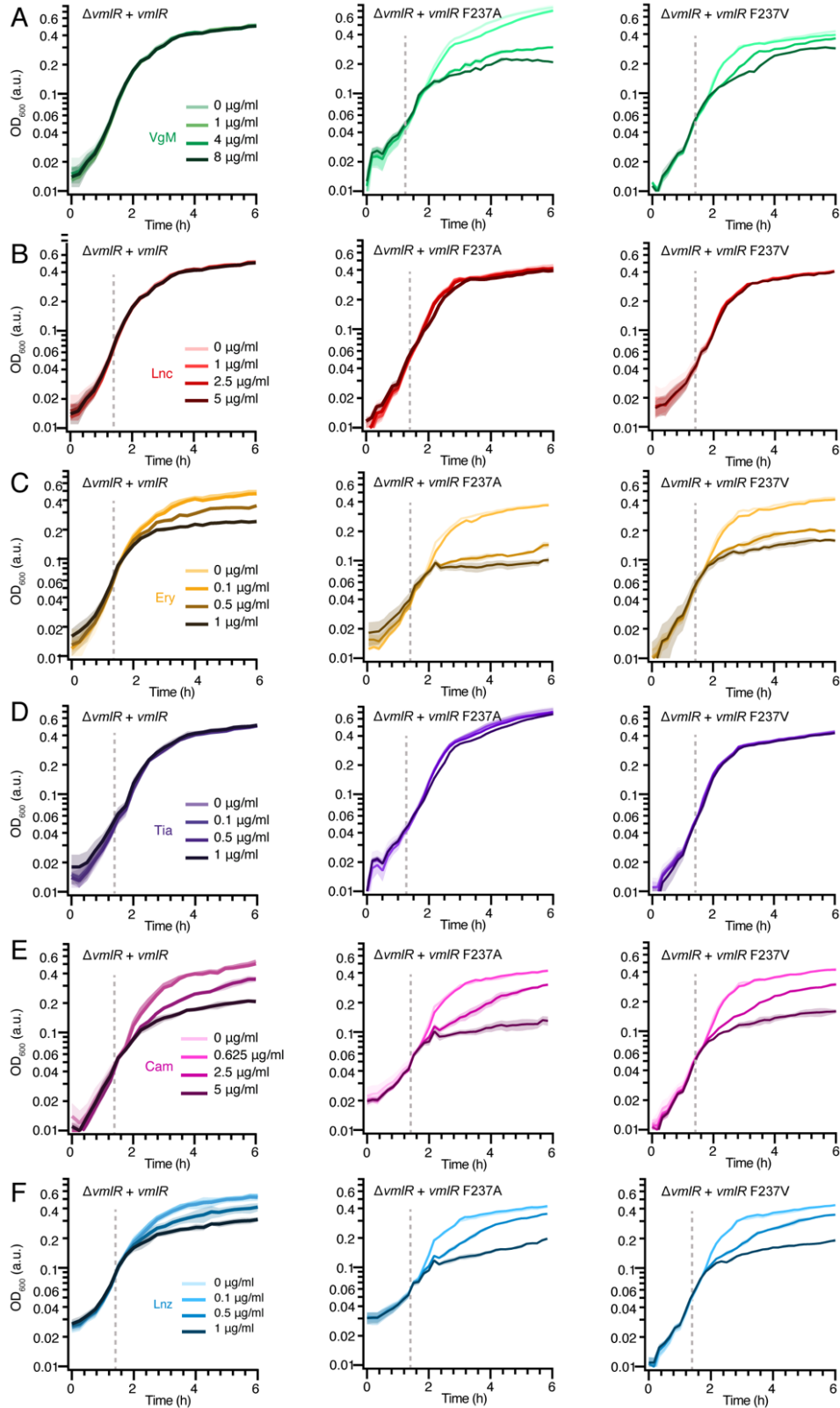


Figure S6. Antibiotic resistance conferred by VmlR variants *in vivo*. (A-F) Growth curves of *vmlR*-knockout ($\Delta vmlR$) complemented by wildtype VmlR ($\Delta vmlR + vmlR$, same panels as in Figure S4), or VmlR variants VmlR-F237A or VmlR-F237V grown in

the presence of increasing concentrations of **(A)** virginiamycin M1 (VgM), **(B)** lincomycin (Lnc), **(C)** erythromycin (Ery), **(D)** tiamulin (Tia), **(E)** chloramphenicol (Cam) and **(F)** linezolid (Lnz). Cells were diluted to an OD₆₀₀ value of 0.01 and grown in LB (with IPTG for the complemented cells) at 37°C with shaking. After 90 minutes antibiotics were added at the indicated concentrations (dashed line) and growth was measured for a further 6 h.

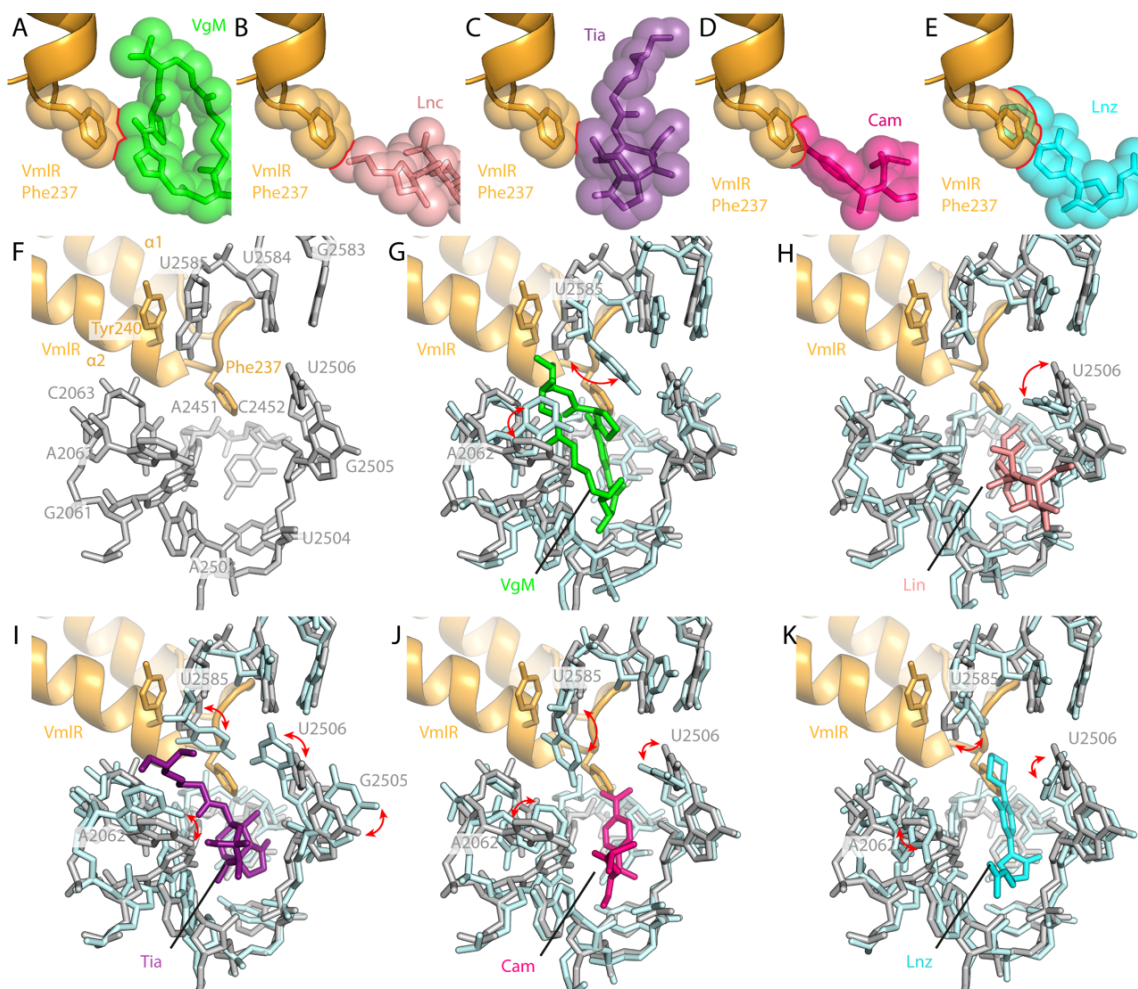


Figure S7. Conformation of the PTC in the presence of VmlR and antibiotics. (A-E) Zoom showing steric clash between Phe237 of VmlR with (A) virginiamycin M (VgM, green), (B) lincomycin (Lnc, salmon), (C) tiamulin (Tia, purple), (D) chloramphenicol (Cam, pink) and (E) linezolid (Lnz, cyan). (F) The conformation of selected 23S rRNA nucleotides (grey sticks) at the PTC in the presence of VmlR (orange). Tyr240 within the ARD of VmlR stacks upon U2585. (G-K) Superimposition of (F) with 23S rRNA nucleotides (cyan) that comprise the binding site of (G) virginiamycin M (VgM, green, PDB ID 1YIT) (25), (H) lincomycin (Lin, pink, PDB ID 5HKV) (26) and (I) tiamulin (Tia, purple, PDB ID 1XBP) (27), (J) chloramphenicol (Cam, pink, PDB ID 4V7U) (28), and (K) linezolid (Lnz, cyan, PDB ID 3DLL) (29). Conformational differences of 23S rRNA nucleotides between VmlR and antibiotic structures are highlighted with red arrows. Note that for (B) lincomycin (Lin, pink, PDB ID 5HKV) (26), the nucleobase of U2585 is not present in the model.

Table S1. Cryo-EM data collection, refinement and validation statistics

	VmlR-SRC (EMD ID EMD-0177, PDB 6HA8)	P-tRNA-SRC (EMD ID EMD-0176, PDB 6HA1)
Data collection		
Microscope	FEI Titan Krios	FEI Titan Krios
Camera	Falcon III	Falcon III
Magnification	131,951	131,951
Voltage (kV)	300	300
Electron dose (e ⁻ /Å ²)	55.5	55.5
Defocus range (µm)	-0.8 to -1.6	-0.8 to -1.6
Pixel size (Å)	1.061	1.061
Initial particles (no.)	159,722	159,722
Final particles (no.)	33,392	68,652
Model composition		
Nonhydrogen atoms	146,414	140,834
Protein residues	6,053	5,300
RNA bases	4,610	4,622
Refinement		
Average resolution (Å)	3.5	3.1
Map CC (around atoms)	0.77	0.79
Map CC (whole unit cell)	0.75	0.79
Map sharpening <i>B</i> factor (Å ²)	-88.20	-88.14
R.m.s. deviations		
Bond lengths (Å)	0.010	0.007
Bond angles (°)	1.3	1.1
Validation		
MolProbity score	1.96 (100 th percentile for structures 3.50Å ± 0.25Å)	1.92 (100 th percentile for structures 3.10Å ± 0.25Å)
Clashscore	7.68 (80 th percentile for structures ≥ 3Å)	7.12 (98 th percentile for structures ≥ 2.85Å)
Poor rotamers (%)	0.87%	0.90%
Ramachandran plot		
Favored (%)	90.36 %	90.67 %
Allowed (%)	9.15 %	8.77 %
Disallowed (%)	0.49 %	0.56 %

Table S2. Primers used for construction of *B. subtilis* strains

VmlR-A-F	CATATGAAATACCGCAAAACAAG
VmlR-A-R	CAATGCCGCTTGAACCTTCTCCC-CCATATCCCTCGCTTAAAGGGAG
VmlR-B-F	GGGAGAAAGTTCAAGCGGCATTG
VmlR-B-R	GCTTGAGTCAATTCCGCTGTCGCATAACGTCAGGAACTTGGACG
VmlR-C-F	CAAAATTAACGTACTGATTGGGTAGGATCCGCGGCTTGAGGATCAGACGCT GATTG
VmlR-C-R	CTGTCCCAGAATGATGTTTCAGTAATG
chpA-R	CGCGGATCCTACCCAATCAGTACGTTAATTTTG
pAPNC-F	CGACAGCGGAATTGACTCAAGC
PhyvmlR_F	CGGATAACAATTAAGCTTAGTCGACGAAGGAGAGAGCGATAATGGCCGGC AAAGAGATCGTAACA
PhyvmlR_R	GTTTCCACCGAATTAGCTTGCATGCTTAGTCTTTTTTGTCTTGATGATCCAGC TCTTTTATTC
pHT002_R	GTCGACTAAGCTTAATTGTTATCCGCTCACAATTACACACATTATGCC
pHT002_F	GCATGCAAGCTAATTCGGTGGAACGAGGTCATC
F237A	CTCAATCGACGAAAAAGGAAGGGGCTAAAGAATATCACCGGGTAAAAG
F237V	TCGACGAAAAAGGAAGGGGTTAAAGAATATCACCGGG
491STOPx2	CAGTTAAACGACGTTCTTCAGAATGATAAGAGCGGGAGGAGC

References

1. Arenz S, *et al.* (2014) Drug sensing by the ribosome induces translational arrest via active site perturbation. *Mol Cell* 56(3):446-452.
2. Arenz S, *et al.* (2014) Molecular basis for erythromycin-dependent ribosome stalling during translation of the ErmBL leader peptide. *Nat Commun* 5:3501.
3. Zheng SQ, *et al.* (2017) MotionCor2: anisotropic correction of beam-induced motion for improved cryo-electron microscopy. *Nat Methods* 14(4):331-332.
4. Zhang K (2016) Gctf: Real-time CTF determination and correction. *J Struct Biol* 193(1):1-12.
5. Kimanius D, Forsberg BO, Scheres SH, & Lindahl E (2016) Accelerated cryo-EM structure determination with parallelisation using GPUs in RELION-2. *Elife* 5.
6. Scheres SH & Chen S (2012) Prevention of overfitting in cryo-EM structure determination. *Nat Methods* 9(9):853-854.
7. Kucukelbir A, Sigworth FJ, & Tagare HD (2014) Quantifying the local resolution of cryo-EM density maps. *Nat Methods* 11(1):63-65.
8. Moriya T, *et al.* (2017) High-resolution single particle analysis from electron cryo-microscopy images using SPHIRE. *J Vis Exp* (123).
9. Chen B, *et al.* (2014) EttA regulates translation by binding the ribosomal E site and restricting ribosome-tRNA dynamics. *Nat Struct Mol Biol* 21(2):152-159.
10. Bienert S, *et al.* (2017) The SWISS-MODEL Repository—new features and functionality. *Nucleic Acids Res* 45(D1):D313-D319.
11. Pettersen EF, *et al.* (2004) UCSF Chimera - A visualization system for exploratory research and analysis. *J Comput Chem* 25(13):1605-1612.
12. Emsley P & Cowtan K (2004) Coot: Model-building tools for molecular graphics. *Acta Crystallographica Section D - Biological Crystallography* 60:2126-2132.
13. Sohmen D, *et al.* (2015) Structure of the *Bacillus subtilis* 70S ribosome reveals the basis for species-specific stalling. *Nat Commun* 6:6941.
14. Fischer N, *et al.* (2015) Structure of the *E. coli* ribosome-EF-Tu complex at <3 Å resolution by C-corrected cryo-EM. *Nature* 520(7548):567-570.
15. Johnson ZL & Chen J (2018) ATP binding enables substrate release from Multidrug Resistance Protein 1. *Cell* 172(1-2):81-89 e10.
16. Rozov A, Demeshkina N, Westhof E, Yusupov M, & Yusupova G (2015) Structural insights into the translational infidelity mechanism. *Nat Commun* 6:7251.
17. Adams PD, *et al.* (2010) PHENIX: a comprehensive Python-based system for macromolecular structure solution. *Acta Crystallogr D Biol Crystallogr* 66(Pt 2):213-221.
18. Chen VB, *et al.* (2010) MolProbity: all-atom structure validation for macromolecular crystallography. *Acta Crystallogr D Biol Crystallogr* 66(Pt 1):12-21.
19. Morimoto T, Ara K, Ozaki K, & Ogasawara N (2011) A simple method for introducing marker-free deletions in the *Bacillus subtilis* genome. *Methods Mol Biol* 765:345-358.

20. Katoh K & Standley DM (2013) MAFFT multiple sequence alignment software version 7: improvements in performance and usability. *Mol Biol Evol* 30(4):772-780.
21. Murina V, Kasari M, Reith M, Hauryliuk V, & Atkinson GC (2017) ABCF ATPases involved in protein synthesis, ribosome assembly and antibiotic resistance: structural and functional diversification across the tree of life. *bioRxiv*: 10.1101/220046. Posted November 16, 2017.
22. Jia B, *et al.* (2017) CARD 2017: expansion and model-centric curation of the comprehensive antibiotic resistance database. *Nucleic Acids Res*:gkw1004.
23. Consortium U (2018) UniProt: the universal protein knowledgebase. *Nucleic Acids Res* 45(5):2699.
24. Karcher A, Schele A, & Hopfner KP (2008) X-ray structure of the complete ABC enzyme ABCE1 from *Pyrococcus abyssi*. *J Biol Chem* 283(12):7962-7971.
25. Tu D, Blaha G, Moore P, & Steitz T (2005) Structures of MLS_BK antibiotics bound to mutated large ribosomal subunits provide a structural explanation for resistance. *Cell* 121(2):257-270.
26. Matzov D, *et al.* (2017) Structural insights of lincosamides targeting the ribosome of *Staphylococcus aureus*. *Nucleic Acids Res* 45(17):10284-10292.
27. Schlunzen F, Pyetan E, Fucini P, Yonath A, & Harms J (2004) Inhibition of peptide bond formation by pleuromutilins: the structure of the 50S ribosomal subunit from *Deinococcus radiodurans* in complex with tiamulin. *Mol Microbiol* 54(5):1287-1294.
28. Dunkle JA, Xiong L, Mankin AS, & Cate JH (2010) Structures of the *Escherichia coli* ribosome with antibiotics bound near the peptidyl transferase center explain spectra of drug action. *Proc Natl Acad Sci U S A* 107(40):17152-17157.
29. Wilson DN, *et al.* (2008) The oxazolidinone antibiotics perturb the ribosomal peptidyl-transferase center and effect tRNA positioning. *Proc Natl Acad Sci U S A* 105(36):13339-13344.